J. Mater. Chem. A

ARTICLE

The way to panchromatic copper(I)-based dye-sensitized solar cells: co-sensitization with the organic dye SQ2

Received 00th January 20xx,
Accepted 00th January 20xx

DOI: 10.1039/x0xx00000x

www.rsc.org/

Frederik J. Malzner,[a] Markus Willgert[a], Edwin C. Constable[a] and Catherine E. Housecroft*[a]

We report the first example of n-type dye-sensitized solar cells (DSCs) co-sensitized with a copper(I)-based sensitizer and an organic dye. The heteroleptic copper(I) dye [Cu(**3**)(**1**)]$^+$ (**3** = anchoring ligand ((6,6'-dimethyl-[2,2'-bipyridine]-4,4'-diyl)bis(4,1-phenylene))bis(phosphonic acid), **1** = ancillary ligand 2-(6-methylpyridin-2-yl)thiazole) was combined with the commercially available squaraine derivative **SQ2**. By prudent matching of the external quantum efficiency (EQE) maxima arising from the two dyes in complementary parts of the visible spectrum, we have achieved the highest photoconversion efficiency reported for a copper-based DSC (65.6% relative to N719 set at 100%). This confirms the potential for the use of Earth-sustainable copper as the basis of sensitizers in DSCs. A combination of *J*–*V* measurements (*J* = current density, *V* = voltage), EQE spectra and electrochemical impedance spectroscopy has been used to optimize and understand the effective use of the co-sensitized DSCs. We have shown that the sequences in which the photoanodes of the n-type DSCs are exposed to [Cu(**3**)(**1**)]$^+$ and **SQ2**, and the times that the electrodes are immersed in the respective dye baths, critically influence the overall performance of the DSCs. A degree of aggregation of the **SQ2** molecules on the electrode surface is important in terms of achieving panchromatic light-harvesting of the co-sensitized DSCs, but excessive aggregation is detrimental.

Introduction

The conversion of solar photons into electrical energy by Grätzel n-type dye-sensitized solar cells (DSCs) is a mature field[1,2,3] with conversion efficiencies reaching ~11–14% using ruthenium-based, organic or zinc(II) porphyrin-based dyes.[4,5,6,7,8,9,10,11,12,13,14,15] Although sensitizers based on ruthenium lead the way among inorganic compounds, the low earth-abundance and high cost of ruthenium are a disadvantage. Among dyes containing sustainable materials,[16] those based on copper are promising alternatives to ruthenium.[17,18,19]

For a good performing DSC, the absorbance of the incident sunlight, the injection of electrons into the semiconductor and the interplay between the dye and the electrolyte must be optimal. The more the absorption range of the dye overlaps with the spectrum of the incident sunlight, the higher the possibility of reaching high conversion efficiencies. The best-performing copper-based dyes achieve >3% photoconversion efficiency (η) relative to values in the range 7.12–7.63% for the benchmark ruthenium dye N719.[20,21,22,23] In contrast to the panchromatic absorption of N719 and related dyes, the metal-to-ligand charge transfer (MLCT) band of copper(I) sensitizers typically lies between ~430 and 570 nm. This range can be broadened by extending the π-system of the copper-bound ligands.[21,24,25,26,27,28] Although this may lead to higher short-circuit current density (J_{SC}) values, it does not necessarily yield enhanced global efficiencies.

Different approaches to panchromatic DSCs have been discussed by Yum *et al.*,[29] and co-sensitization with dyes which absorb in complementary parts of the visible spectrum is a favoured approach.[30,31,32,33] By co-sensitization of N719 with a porphyrin-dye, Chang *et. al.*[31] obtained enhanced absorption between 600 and 700 nm with respect to N719, and reached a higher J_{SC} (18.51 *versus* 16.41 mA cm^{-2}) and a higher η (8.89 *versus* 8.02%). However, co-sensitization does not always lead to improved DSC performance. A cocktail of organic and {Ru^{II}(bpy)$_2$(NCS)$_2$}-based dyes reported by Babu *et. al.*[30] performed marginally less efficiently than the ruthenium dye alone (η = 9.20 versus 9.26%). The use of squaraine dyes, in particular **SQ2** (Scheme 1), as co-sensitizers with various organic dyes has been investigated.[32,34,35,36,37,38,39,40] Depending on the organic dye combined with **SQ2**, values of η up to 8.14%[40] have been obtained, representing an overall improvement of 37% with respect to a DSC containing only the organic dye. **SQ2** was first synthesized and used as a dye for DSCs by Geiger *et. al.*[41] and is now available commercially (Solaronix SA, Aubonne, Switzerland).

[a] *Department of Chemistry, University of Basel, Spitalstrasse 51, CH-4056 Basel, Switzerland; email: catherine.housecroft@unibas.ch*

†Electronic Supplementary Information (ESI) available: Table S1: Performance data for duplicate DSCs; Fig. S1–S9: Additional J–V curves and EQE spectra. See DOI: 10.1039/x0xx00000x

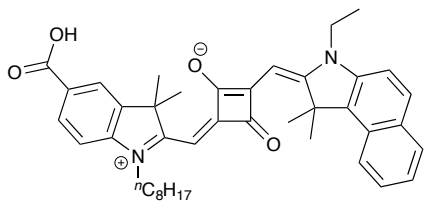

SQ2

Scheme 1 The organic squaraine co-sensitizer **SQ2** used in this study.

To combine sensitizers in a DSC, different methods and sequences of applying the dyes to the semiconductor surface have been used.[37,39,42] Xue *et. al*.[37] arranged discrete dye layers onto a plastic surface by stepwise deposition of TiO_2 nanoparticles and dye. Rudolph *et. al*.[39] investigated various procedures to absorb dyes individually or in different combinations with the help of dye-baths. Dyes can also be applied to the TiO_2 surface by inkjet printers.[42]

Our current interest in copper(I) bis(diimine) dyes[17] has led to values of η > 3%,[20,22,23] representing 40-50% of the photoconversion efficiency of N719 in DSCs with a similar configuration. We now report the first co-sensitization of a copper(I)-based DSC with a complementary organic dye in order to significantly enhance DSC photoconversion efficiency.

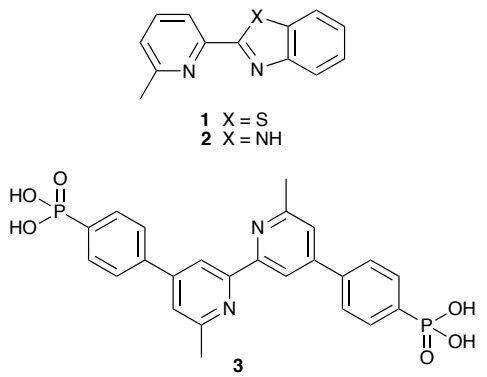

1 X = S
2 X = NH

3

Scheme 2 Structures of ancillary ligands **1** and **2** and anchoring ligand **3** for copper(I) co-sensitized DSCs from Ref. 44.

Experimental

General

Ligands **1**[22] and **3**[43] (Scheme 2) were prepared as previously reported. **SQ2** and N719 were purchased from Solaronix. Solid-state absorption spectra were recorded on an Agilent Cary 5000 spectrophotometer.

Ground state density functional theory (DFT) calculations were performed using Spartan 16 (v. 1.1.1, Wavefunction Inc.) at the B3LYP level with a 6-31G* basis set in vacuum. Initial energy optimization was carried out at a semi-empirical (PM3) level.

DSC fabrication and measurements

Solvents were HPLC grade except for DMSO (extra dry). Commercial Solaronix Test Cell Titania Electrodes were washed with EtOH and sintered at 450 °C for 30 min. After cooling to ~80 °C, the electrodes were dipped in dye-baths according to the dipping procedures described in the Results and discussion section. After the first dipping step (see discussion), the electrodes were washed with DMSO and EtOH and dried with a heat gun (~ 80 °C). CH_2Cl_2 was used to wash the electrodes after the second and third dipping steps (see discussion) and the electrodes were finally dried with a heat gun (~80 °C). An N719 reference electrode was prepared by dipping a Solaronix Test Cell Titania Electrode in a solution of N719 (0.3 mM, EtOH, ambient temperature) for 3 days. After removal from the dye-bath, the electrode was washed with EtOH and dried with a heat gun (~80 °C).

For the counter electrodes, Solaronix Test Cell Platinum Electrodes were used. Before assembling the DSCs, the counter electrodes were washed with EtOH and placed on a heating plate (450 °C, 30 min) in order to remove volatile organic impurities.

The photoanode and the counter electrode were joined using thermoplast hot-melt sealing foil (Solaronix Test Cell Gaskets) by heating while pressing them together. The electrolyte (electrolyte composition: LiI (0.1 M), I_2 (0.05 M), 1-methylbenzimidazole (0.5 M), 1-butyl-3-methylimidazolinium iodide (0.6 M) in 3-methoxypropionitrile) was introduced into the DSC by vacuum backfilling. The hole in the counter electrode was sealed (Solaronix Test Cell Sealings) and covered (Solaronix Test Cell Caps.)

Measurements were made by irradiating from behind using a light source SolarSim 150 (1000 W m^{-2} = 100 mW cm^{-2} = 1 sun). The power of the simulated light was calibrated by using a reference Si photodiode. All cells were completely masked[44,45] before measurements were made. A series of masks with calibrated apertures was used; the area of each was accurately known and was in the range 0.059–0.061 cm^2. *J-V* curves of the DSCs with light-blocking filters (THORLABS, 25mm sputtered edgepass filter, short-pass 500 nm; Reichmann Feinoptik, Farbglasfilter OG 550, long-pass 550 nm; Andover Corporation, 41% transmittance filter) were obtained by placing the filter on top of the fully-masked DSC. The light intensity was measured by placing the filter on top of a fully-masked reference Si photodiode. For the filter test measurements, the best performing single-dye **SQ2** DSC at day 195 after assembling the cell and a co-sensitized DSC assembled by *Experiment 4* procedure (see discussion section) on day 72 after assembling the cell were used.

The external quantum efficiency (EQE) measurements were made using a Spe-Quest quantum efficiency instrument from Rera Systems (Netherlands) equipped with a 100 W halogen lamp (QTH) and a lambda 300 grating monochromator (Lot Oriel). The monochromatic light was modulated to 3 Hz using a chopper wheel (ThorLabs). The cell response was amplified with a large dynamic range IV converter (CVI Melles Griot) and then measured with a SR830 DSP Lock-In amplifier (Stanford Research). EQE spectra of single-dye DSCs and co-sensitized DSCs were performed after calibrating the system with a reference cell. Measurements with a 500 nm short-pass filter and the combined 500 nm short-pass and 550 nm long-

pass filter were performed under the same calibration. The EQE spectra with a 550 nm long-pass filter were obtained after calibration with the 550 nm long-pass filter on top of the reference cell. In all EQE measurements with a filter, the filter was placed on top of the bias light in order to filter only the incoming EQE light beam. The same DSCs as in the *J-V* measurements with filters were used for the EQE measurements.

Electrochemical impedance spectroscopy (EIS) measurements were carried out on a ModuLab® XM PhotoEchem photoelectrochemical measurement system from Solartron Analytical. The impedance was measured in galvanostatic mode at open-circuit potential of the cell at different light intensities (590 nm) in the frequency range 0.05 Hz to 400 kHz using an amplitude of 10 mV. The impedance data were analysed using ZView® software from Scribner Associates Inc.

Electrodes for solid-state absorption spectroscopy

Dye-functionalized electrodes were prepared using Solaronix Test Cell Titania Electrodes Transparent. The electrodes were washed with EtOH and sintered at 450 °C. For the [Cu(**3**)(**1**)]$^+$-functionalized surface, the post-sintered electrode was cooled to ~80 °C and then dipped into a DMSO solution of ligand **3** (1 mM) for 24 h. Then the electrode was washed with DMSO and EtOH and dried with a heat gun (~80 °C). The electrode was then dipped into a CH_2Cl_2 solution of [Cu(**1**)$_2$][PF_6] (0.1 mM) for 3 d. After removal from the dye-bath, the electrode was washed with CH_2Cl_2 and dried with a heat gun (~80 °C). For the **SQ2**-funtionalized electrode, the post-sintered electrode was cooled to ~80 °C and was dipped into a CH_2Cl_2 solution of **SQ2** (0.1 mM) for 20 min. Then the electrode was washed with CH_2Cl_2 and dried with a heat gun (~80 °C).

Results and discussion

Selection of the dyes for panchromatic co-sensitized DSCs

We have reported the performances of DSCs sensitized with heteroleptic [Cu(**3**)($L_{ancillary}$)]$^+$ complexes where $L_{ancillary}$ was 2-(1H-imidazol-2-yl)-6-methylpyridine (**2**, Scheme 2), 2-(6-methylpyridin-2-yl)oxazole, 2-(6-methylpyridin-2-yl)thiazole (**1**, Scheme 2) or 2-methyl-6-(1-methyl-1H-imidazol-2-yl)pyridine) and using an I^-/I_3^- redox couple.[22] The heteroleptic dyes were assembled on FTO/TiO_2 electrodes using our stepwise 'surface-as-ligand' approach (Scheme 3).[17] Although the dye with ancillary ligand **2** produced the highest open-circuit voltage (V_{OC} = 608 mV), use of **1** gave the highest J_{SC} (7.76 mA cm^{-2}). The global efficiencies of the best performing DSCs with [Cu(**3**)(**2**)]$^+$ and [Cu(**3**)(**1**)]$^+$ were 3.03 and 2.88% on the day that the devices were fabricated *versus* 7.55% for the reference dye N719 (Table 1). The dye-assembly procedure (Scheme 3) relies upon the use of a homoleptic complex [Cu($L_{ancillary}$)$_2$][PF_6], and [Cu(**1**)$_2$][PF_6] proved to be more air-stable in solution than [Cu(**2**)$_2$][PF_6]. Thus, for the present study, we chose to use ancillary ligand **1**.

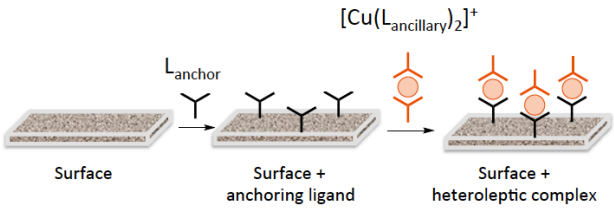

Scheme 3 Stepwise 'surface-as-ligand' assembly of heteroleptic copper(I) dyes in n-type DSCs. In [Cu(**3**)(**1**)]$^+$, L_{anchor} = **3** and $L_{ancillary}$ = **1**.

Although previously reported,[22] it is convenient for our discussion to provide the performance parameters of DSCs containing [Cu(**3**)(**1**)]$^+$ combined with an I_3^-/I^- electrolyte (Table 1). Fig. S1† displays the *J-V* curves on the day of sealing the cells, and 3 and 7 days later. The external quantum efficiency (EQE) spectra exhibit a maximum at 480 nm (Fig. S2†). The photoconversion efficiency of 2.88% *versus* 7.55% for N719 (Table 1) is relatively high for a copper(I) sensitizer.[17,22]

Table 1 Performance parameters and EQE maxima of a DSC containing the dye [Cu(**3**)(**1**)]$^+$. Data are taken from ref. 22 and are reproduced here for convenience

Dye	J_{SC} [mA cm^{-2}]	V_{OC} [mV]	*FF* [%]	η [%]	Rel. η[a] [%]	EQE max. [nm], [%]
On the day of sealing the cell (Day 0)						
[Cu(**3**)(**1**)]$^+$	7.76	530	69.9	2.88	38.1	480, 53.8
N719	16.57	630	72.4	7.55	100	540, 71.8
Day 3						
[Cu(**3**)(**1**)]$^+$	6.77	542	70.4	2.58	35.8	480, 50.8
N719	15.03	660	72.6	7.21	100	520, 70.8
Day 7						
[Cu(**3**)(**1**)]$^+$	7.42	558	62.6	2.59	37.7	470, 46.2
N719	14.47	650	73.0	6.87	100	540, 71.1

[a]Rel. η is the efficiency relative to an N719 reference which is set at 100%.

The squaraine dye **SQ2**[35,36,37,39,40,41] (Scheme 1) was chosen as co-sensitizer because the absorption range complements that of [Cu(**3**)(**1**)]$^+$. The solid-state UV-Vis spectra of dye-functionalized FTO/TiO_2 surfaces with the two separate dyes are shown in Fig. 1 and demonstrate the wavelength range between 375 and 730 nm covered by the dyes. Several studies of DSCs sensitized by **SQ2** have been reported and Table 2 summarizes the results.[34,35,36,38,40,41] However, the use of CH_2Cl_2 as the **SQ2** dye-bath solvent has not been reported. For copper-based dyes, CH_2Cl_2 is an optimal solvent for the homoleptic complex[46] and we were interested to find out whether this solvent was also appropriate for fabrication of DSCs containing **SQ2**. DSCs with **SQ2** and an I^-/I_3^- redox shuttle were assembled as described in the Experimental section. Table 3 displays the performance parameters of these devices, made using different dipping times of the photoanodes in the dye-bath before fabrication of the devices. Despite the use of a different dye-bath solvent, the performances compare well with literature data (Table 2 *versus* Table 3). It is observed that with CH_2Cl_2 as the dye-bath solvent, higher J_{SC} values can be obtained (up to 12.24 mA cm^{-2}), but V_{OC} values are lower compared to those in Table 2. It is significant that n-type DSCs

containing the **SQ2** dye exhibit photoconversion efficiencies (2.62% to 3.28%, Table 3) which are comparable to those of DSCs sensitized with $[Cu(\mathbf{3})(\mathbf{1})]^+$ (2.88%, Table 1).

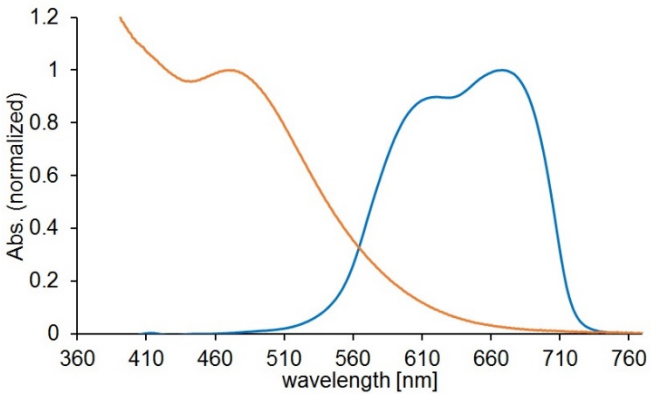

Fig. 1. Solid-state absorption spectra of FTO/TiO_2 electrodes functionalized with the copper(I)-dye $[Cu(\mathbf{3})(\mathbf{1})]^+$ (orange) or the organic-dye **SQ2** (blue) (normalized to the absorption maximum of the respective dye). The high-energy tail is the absorption of the TiO_2.

Table 2 Performance parameters of DSCs containing the dye **SQ2** in literature compared to reference dye N719. In each case, an I^-/I_3^--based electrolyte was used.

Dye	Solvent	J_{SC} [mA cm^{-2}]	V_{OC} [mV]	*FF* [%]	η [%]	η_{N719} [%]	Ref.
SQ2	MeCN : *t*-BuOH : DMSO (3.5 : 3.5 : 3)	11.05	600	60	3.98	7.97	34
SQ2	MeCN : *t*-BuOH (1:1)	10.38	600	66	4.11	-[a]	35
SQ2	MeCN : *t*-BuOH (1:1)	9.96	600	64	3.81	8.41	36
SQ2	MeCN : *t*-BuOH (1:1)	9.88	632	69	4.28	-[a]	38
SQ2	EtOH	9.00	640	72	4.16	-[a]	41
SQ2	THF	10.33	570	64	3.78	8.61	40

a) Not reported

Table 3 Performance parameters and EQE maxima of DSCs containing the dye **SQ2** with different dipping times of the photoanodes in the dye-bath before fabrication of the devices

Dye	Dipping time	J_{SC} [mA cm^{-2}]	V_{OC} [mV]	*FF* [%]	η [%]	Rel. η[a] [%]	EQE max. [nm], [%]
On the day of sealing the cell (Day 0)							
SQ2	20 min	6.99	521	71.9	2.62	34.7	670, 44.4
SQ2	2 h	7.91	491	67.4	2.62	34.7	580, 48.6
SQ2	4 h	9.46	504	68.7	3.28	43.4	560, 51.5
SQ2	24 h	9.44	494	68.0	3.17	42.0	560, 51.0
SQ2	3 d	8.32	503	68.0	2.85	37.7	560, 47.5
N719	1 d	16.57	630	72.4	7.55	100	540, 71.8
Day 7							
SQ2	20 min	9.18	531	69.8	3.40	49.5	660, 49.2
SQ2	2 h	10.73	529	66.5	3.77	54.9	560, 57.6
SQ2	4 h	11.84	544	68.9	4.44	64.6	550, 59.6
SQ2	24 h	12.24	529	66.8	4.32	62.9	550, 58.9
SQ2	3 d	10.95	529	67.2	3.89	46.6	550, 54.6
N719	1 d	14.47	650	73.0	6.87	100	540, 71.1

[a]Rel. η is the efficiency relative to an N719 reference which is set at 100%.

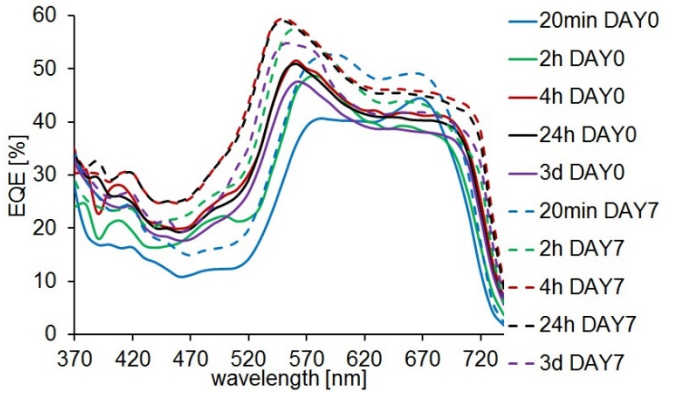

Fig. 2 EQE curves of a DSC containing the dye **SQ2** with different dipping times of the photoanodes in the dye-bath before fabrication of the devices.

The previously reported influence of aggregation of **SQ2** on the semiconductor surface and the impact on performance[34,35,36,37,38,39,40,41] was also observed in our study. Longer dipping times lead to more aggregation resulting in a broader EQE spectrum, and a shift in the EQE maximum from 670 to 560 nm (Fig. 2 and Table 3). Extensive aggregation of **SQ2** molecules on the surface leads to greater quenching of the excited state of the dye and a lower recombination resistance (R_{rec}) at the TiO_2/dye/electrolyte-interface (see later). This results in lower J_{SC} values.[34,35,36,37,38,39,40,41] However, some degree of aggregation is beneficial, leading to a broader absorption range and improved J_{SC} values. Fig. 2 demonstrates that a dipping time of 4 hours results in an optimum EQE curve on the day of cell fabrication, and longer dipping times lead to a decrease in DSC performance (Table 3). Inspection of Fig. 3 and Table 3 confirms the influence of the dipping time in the **SQ2** dye-bath on J_{SC} and the overall cell performance. Significantly, there is a pronounced ageing effect, which is observed both in the EQE (Fig. 2) and the *J*–*V* curves (Fig. 3). After the DSCs had been stored in the dark for 7 days, a maximum value of η = 4.44% (*versus* 6.87% for N719) was obtained (Table 3).

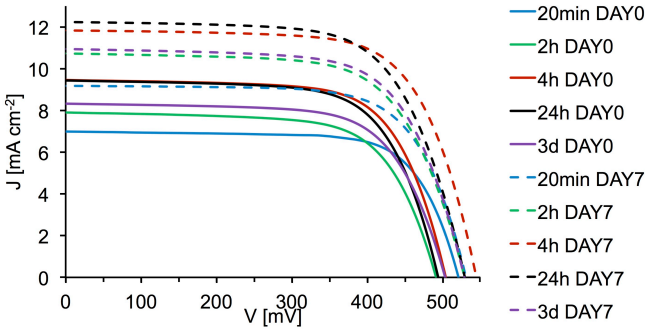

Fig. 3 *J*-*V* curves of a DSC containing the dye **SQ2** with different dipping times of the photoanodes in the dye-bath before fabrication of the devices.

The structural differences between a phosphonic acid anchor (as in **3**) and a carboxylic acid (as in **SQ2**) lead to different modes of bonding to the TiO_2 surface.[47,48,49,50] It is also known that phosphonic acids bind more strongly to metal oxide surfaces than carboxylic acids.[47] We anticipated that

both dyes could be absorbed simultaneously onto the semiconductor surface, but needed to establish a methodology for optimal co-sensitization of the electrodes.

Investigation of the optimal dipping procedure for co-sensitized DSCs

The goal of this part of the investigation was to optimize the EQE response for DSCs co-sensitized with $[Cu(\mathbf{3})(\mathbf{1})]^+$ and **SQ2**. The assembly of the heteroleptic $[Cu(\mathbf{3})(\mathbf{1})]^+$ using our 'surface-as-ligand' approach[17] requires that the photoanode is first immersed in a solution of anchoring ligand **3**. In a second step, the functionalized photoanode is dipped into a CH_2Cl_2 solution of the homoleptic complex $[Cu(\mathbf{1})_2][PF_6]$. After ligand exchange (Scheme 3), $[Cu(\mathbf{3})(\mathbf{1})]^+$ is bound to the semiconductor surface. Different dipping procedures were investigated to reach comparable values of EQE_{max} for DSCs containing both dyes. Table 4 summarizes the different dipping procedures with the sequences in which the photoanode was sequentially immersed into the dye-baths. Fig. 4 displays the stepwise dipping procedure of photoanodes, exemplifed by the procedure for *Experiment 2* in Table 4. For the screening of dipping conditions, one DSC for each set of conditions was used.

Table 4 Investigated dipping procedures with anchoring ligand **3**, homoleptic complex $[Cu(\mathbf{1})_2][PF_6]$ and the organic dye **SQ2**.

Experiment number	1st dipping step	2nd dipping step	3rd dipping step
1	**3**[a]	**SQ2** (time = *x*[b])	$[Cu(\mathbf{1})_2][PF_6]$[c]
2	**3**[a]	$[Cu(\mathbf{1})_2][PF_6]$[c]	**SQ2** (time = *x*[b])
3	**3** : **SQ2** (1:1) concentrations[d]	$[Cu(\mathbf{1})_2][PF_6]$[c]	- - -
4	**3** : **SQ2** (1:1) concentrations[e]	$[Cu(\mathbf{1})_2][PF_6]$[c]	**SQ2** (20 min)[f]

a) Dye-bath solvent: DMSO; concentration: 1 mM; dipping time: 1 d

b) Dye-bath solvent: CH_2Cl_2; concentration: 0.1 mM; dipping time: *x* = 20 min, 1 h, 2 h, 4 h

c) Dye-bath solvent: CH_2Cl_2; concentration: 0.1 mM; dipping time: 3 d

d) Dye-bath solvent: **3** in DMSO, **SQ2** in CH_2Cl_2; concentration: **3**: 0.1 mM, **SQ2**: concentration = 0.1 mM, 0.01 mM, 0.001 mM or 0.0001 mM; dipping time: 1 d

e) Dye-bath solvent: **3** in DMSO, **SQ2** in CH_2Cl_2; concentration: **3**: 0.1 mM, **SQ2**: concentration = 0.1 mM, 0.01 mM, 0.001 mM or 0.0001 mM; dipping time: 1 d

f) Dye-bath solvent: CH_2Cl_2; concentration: 0.1 mM; dipping time: 20 min

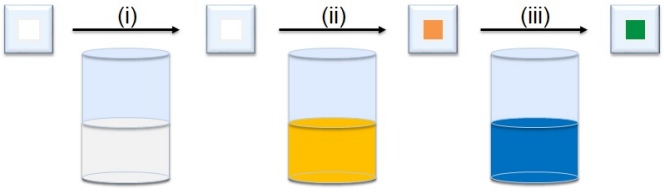

Fig. 4 Stepwise dipping procedure of photoanodes with the dipping procedure of *Experiment 2* (Table 4) starting with (i) the colourless solution of anchoring ligand **3**, (ii) followed by the orange-coloured homoleptic $[Cu(\mathbf{1})_2][PF_6]$ dye-bath solution and (iii) the blue-coloured **SQ2** dye-bath in the third dipping step resulting in green coloured photoanodes.

Fig. S3–S6† display the EQE spectra of all DSCs described in Table 4, and Fig. 5 shows the EQE spectra of the DSCs with the best EQE response of the several dipping procedures in Table 4. The four experiments in Table 4 explore the effects of introducing anchoring ligand **3** and dye **SQ2** sequentially or together, and also the effects of employing a second immersion of the electrodes in a solution of **SQ2**. Irrespective of the dipping procedure, the EQE spectrum shows a maximum at 480 nm associated with the copper(I)-dye and at this wavelength, EQE_{max} is between 46.0 and 49.5% (Table 5). This compares to 54% (Table 1) for a DSC with the copper(I)-dye on its own. However, the electrode-assembly protocol has a significant impact on the EQE response between 560 and 730 nm arising from adsorbed **SQ2**. Values of EQE_{max} range from 3.0 to 57.1%, and latter compares to the highest value of 51.5% for a DSC containing only **SQ2** (Table 3, day 0). We note that in each of the four experiments in Table 4, the individual EQE spectra have the same shape of curve (Fig. S3–S6†) but the intensity varies.

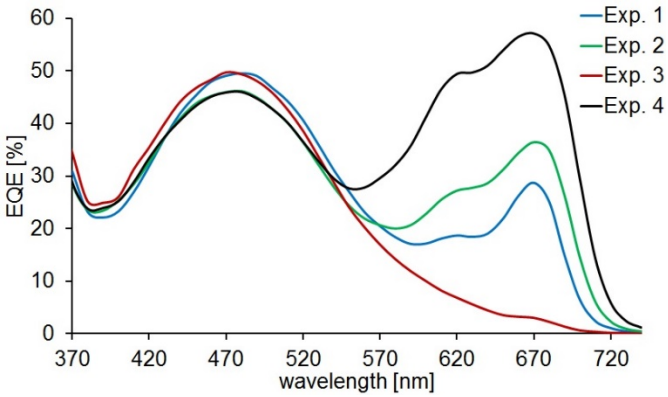

Fig. 5 EQE curves of the DSCs with the best EQE response for the different dipping procedures at the day of sealing the cell.

The best EQE response in *Experiment 1* (defined in Table 4) was measured with a dipping time of **SQ2** of 2 hours. In the third dipping step, the $[Cu(\mathbf{1})_2][PF_6]$ dye-bath was initially orange but during the time that the electrode was in the bath, the colour of the solution changed from orange to greenish. This suggests that **SQ2** (which is blue) is partly washed off the surface. Fig. 5 and S3† show that for *Experiment 1*, the EQE response of **SQ2** is low (EQE_{max} = 28.7%, Table 5) and has the narrow shape characteristic of the solution UV-Vis spectrum of **SQ2** (Fig. S7†).[34,35,38,39,41] This indicates that there is little aggregation of **SQ2** on the surface. The copper(I)-dye $[Cu(\mathbf{3})(\mathbf{1})]^+$ has a good EQE response with a maximum of 49.5% at λ_{max} = 480 nm (Table 5).

Table 5 EQE maxima of **SQ2** and $[Cu(\mathbf{3})(\mathbf{1})]^+$, respectively, of the DSCs with the best EQE response for the different dipping procedures at the day of sealing the cell. See also Fig. 5.

Experiment number	EQE max. of **SQ2** [%], [nm]	EQE max. of $[Cu(\mathbf{3})(\mathbf{1})]^+$ [%], [nm]
1	28.7, 670	49.5, 480
2	36.4, 670	46.1, 480
3	3.0, 670	49.7, 470
4	57.1, 670	46.0, 480

In *Experiment 2* (defined in Table 4), the sequence of the second and third dipping steps was changed with respect to *Experiment 1*. First the heteroleptic copper(I)-dye $[Cu(\mathbf{3})(\mathbf{1})]^+$ was assembled on the TiO_2 surface by sequential exposure to anchor **3** and then $[Cu(\mathbf{1})_2][PF_6]$ (Scheme 3). In the third dipping step, **SQ2** was applied to the photoanode (Fig. 4). The EQE response due to the copper(I)-based dye (EQE_{max} = 46.1% at λ_{max} = 480 nm is similar to that in *Experiment 1* (Table 5 and Fig. 5). However, more **SQ2** is present on the surface with respect to *Experiment 1*. This results in more aggregation and a broader and higher EQE curve between 580 and 720 nm (Fig. 5). The same trend in aggregation as in single-dye **SQ2** DSCs (Fig. 2) was also observed in *Experiment 2* (Fig. S4†). The longer the dipping time, the more aggregation is observed. The benefit of a certain level of aggregation (discussed earlier) is observed on increasing the dipping time from 20 minutes to 2 hours (at λ_{max} = 670 nm, EQE_{max} rises from 33.1 to 36.8%). However, a longer dipping time of 4 hours results in higher aggregation and a low EQE_{max} of 28.7%. The best EQE response in *Experiment 2* was obtained by a cell with a dipping time of **SQ2** of 1 hour.

Experiments 1 and *2* demonstrate that some degree of aggregation of **SQ2** on the TiO_2 surface is important in order to achieve a panchromatic DSC. In order to optimize the aggregation of **SQ2**, the organic dye was introduced with different concentrations (0.0001 to 0.1 mM) to the anchoring ligand solution (0.1 mM) in the first dipping step (*Experiments 3* and *4*). The very low concentrations of **SQ2** were used because of the higher extinction coefficient of **SQ2** with respect to the MLCT band of $[Cu(\mathbf{3})(\mathbf{1})]^+$. In *Experiment 3* (defined in Table 4), only a second dipping step with the homoleptic $[Cu(\mathbf{1})_2][PF_6]$ was applied. The same problem as was encountered in *Experiment 1* was observed. Dye **SQ2** anchored in the first immersion step was partly washed off during the second dipping cycle. Only the DSC with the highest **SQ2** concentration in the first dipping step (0.1 mM) showed a visible EQE response (EQE_{max} = 3.0%) at λ_{max} = 670 nm (Table 5 and Fig. 5). Interestingly, the value of EQE_{max} of the copper(I)-dye (49.7%) in *Experiment 3* is as high as in *Experiment 1* (Table 5) in which **SQ2** was not present in the first dipping step. This is consistent with both **3** and **SQ2** being able to bind simultaneously to the TiO_2 surface.

In *Experiment 4* (defined in Table 4) a final dipping step in which the electrode was exposed to **SQ2** for a second time was introduced. The aim was to refill the surface-vacancies created through loss of **SQ2** in the second dipping step (see above). Because of the introduction of **SQ2** in the first dipping step, more binding sites for **SQ2** are available and more aggregation can take place. This effect is visible in all measured DSCs of *Experiment 4* (Fig. S6†) in comparison to *Experiment 3*.

The best panchromatic EQE response was recorded with a device from *Experiment 4* with an **SQ2** concentration of 0.01 mM in the first dipping step (black curve in Fig. 5). Values of EQE_{max} = 57.1% (λ_{max} = 670 nm) for **SQ2** and EQE_{max} = 46.0% (λ_{max} = 480 nm) from $[Cu(\mathbf{3})(\mathbf{1})]^+$ were observed. The presence of **SQ2** in the first dipping step leads to more anchored **SQ2** on the final photoanode. In addition, the solubility of ligand **3** is an important parameter; **3** is poorly soluble in CH_2Cl_2 and some precipitation is observed when the CH_2Cl_2 solution of **SQ2** is added to the DMSO solution of **3**.

In conclusion, the optimized EQE spectral response with matched values of EQE_{max} at 480 and 670 nm was obtained using the dipping procedure in *Experiment 4* with the following sequence of steps: (i) **3** in DMSO (0.1 mM) and **SQ2** in CH_2Cl_2 (0.01 mM) for 1 day, (ii) $[Cu(\mathbf{1})_2][PF_6]$ in CH_2Cl_2 (0.1 mM) for 3 days, and (iii) **SQ2** in CH_2Cl_2 (0.1 mM) for 20 min. This result was validated using four DSCs.

Performances of panchromatic co-sensitized DSCs

This part of the investigation deals with the performance and properties of co-sensitized DSCs assembled by the dipping procedure of *Experiment 4* (Table 4) with an **SQ2** concentration of 0.01 mM in the dye-bath of the first dipping step. Measurements were performed using duplicate (two), fully-masked DSCs (Table S1†) with an I_3^-/I^- electrolyte (see Experimental section). On the day of sealing the DSCs, the duplicate devices both achieved high values of J_{SC} (10.18 and 9.56 mA cm^{-1}) and similar overall efficiences (3.67 and 3.36% *versus* 7.55% for N719). Ageing of both cells over a period of a week led to enhanced values of J_{SC}, V_{OC} and η (Tables 6 and S1†). In the following discussion, we focus on the better performing DSC of the set. Table 6 also shows the device parameters of this DSC, of single-dye DSCs and of a reference cell containing N719.

The initial value of J_{SC} for the co-sensitized DSC (9.56 mA cm^{-2}, Table 6) is higher than that of the single-dye DSCs (7.76 mA cm^{-2} for $[Cu(\mathbf{3})(\mathbf{1})]^+$ and 6.99 mA cm^{-2} for **SQ2**). The V_{OC} of 493 mV is lower than single-dye DSCs (530 mV for $[Cu(\mathbf{3})(\mathbf{1})]^+$ and 521 mV for **SQ2**), while the fill factor (*FF*) remains high (71.2%). The η of this device is 3.36% relative to 7.55% for N719. Fig. 6 displays the *J–V* curves of the co-sensitized device on the day of cell fabrication and after ageing; a comparison with single-dye DSCs is shown in Fig. S8†. The EQE spectra of the device are shown in Fig. 7 and a comparison with the single-dye DSCs is made in Fig. S9†.

Table 6. Performance parameters and EQE maxima of single-dye DSCs containing the dye [Cu(**3**)(**1**)]$^+$ (data are taken from ref. 22) and **SQ2** with a dipping time of 20 minutes and the best-performing co-sensitized DSC on the day of sealing the cell, 3 days and 7 days later. See Table S1† for data for duplicate DSCs.

Dye	J_{SC} [mA cm^{-2}]	V_{OC} [mV]	*FF* [%]	η [%]	Rel. η[a] [%]	EQE max. [nm], [%]	
On the day of sealing the cell (Day 0)							
[Cu(**3**)(**1**)]$^+$	7.76	530	69.9	2.88	38.1	480, 53.8	
SQ2	6.99	521	71.9	2.62	34.7		670, 44.4
co-sens. DSC	9.56	493	71.2	3.36	44.5	480, 46.0	670, 57.1
N719	16.57	630	72.4	7.55	100	540, 71.8	
Day 3							
[Cu(**3**)(**1**)]$^+$	6.77	542	70.4	2.58	35.8	480, 50.8	
SQ2	9.25	537	69.5	3.45	47.9		670, 47.5
co-sens. DSC	11.86	515	71.9	4.39	60.9	480, 46.3	670, 58.1
N719	15.03	660	72.6	7.21	100	520, 70.8	
Day 7							
[Cu(**3**)(**1**)]$^+$	7.42	558	62.6	2.59	37.7	470, 46.2	
SQ2	9.18	531	69.8	3.40	49.5		660, 49.2
co-sens. DSC	12.26	515	71.3	4.51	65.6	480, 47.1	670, 59.3
N719	14.47	650	73.0	6.87	100	540, 71.1	

[a]Rel. η is the efficiency relative to an N719 reference which is set at 100%.

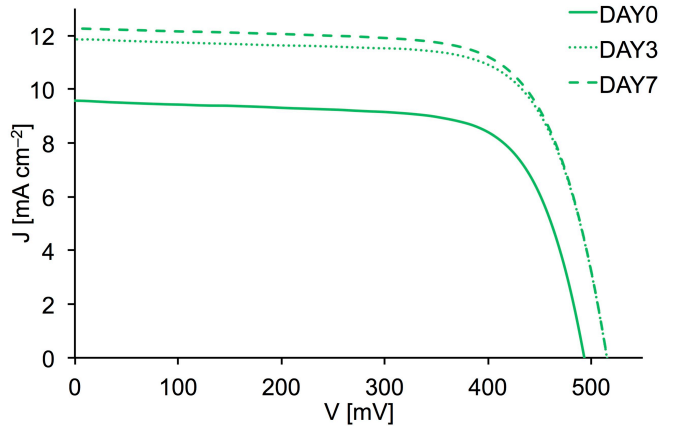

Fig. 6 J-V curves of the best performing co-sensitized DSC assembled with the dipping procedure of Experiment 4 and a SQ2-concetration of 0.01 mM in the first dipping step on the day of sealing the cell (DAY0), 3 days and 7 days later.

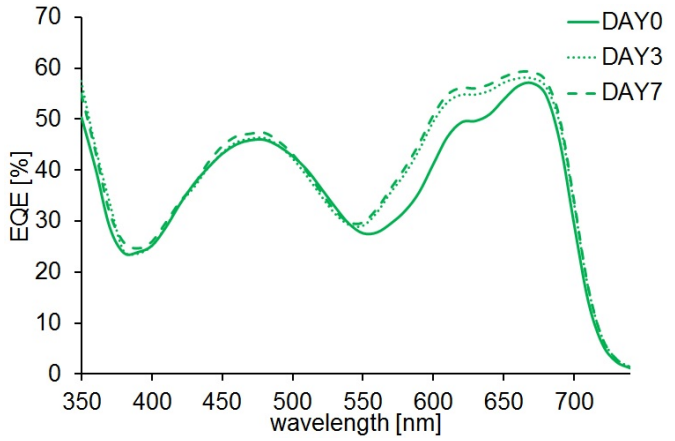

Fig. 7 EQE curves of the best performing co-sensitized DSC assembled with the dipping procedure of *Experiment 4* and a **SQ2**-concentration of 0.01 mM in the first dipping step on the day of sealing the cell (DAY 0), 3 days and 7 days later.

The increase in J_{SC} over a 7 day period after cell fabrication (Fig. 6) is a known phenomenon and most probably arises from reorganization of the dye molecules on the TiO_2 semiconductor surface.[51,52,53] The EQE maxima of both dyes in the co-sensitized cell also increase over a period of 7 days, but this is more pronounced for **SQ2** (Fig. 7). The value of EQE_{max} at λ_{max} = 480 nm (copper(I)-based dye) increases from 46.0% to 47.1% (Table 6). The EQE maximum at λ_{max} = 670 nm (from **SQ2**) increases from 57.1% to 59.3% over a period of 7 days and a higher level of aggregation results in a broader and higher EQE response between 540 and 740 nm (Fig. 7).[34,35,36,37,38,39,40,41] We note that the dipping times in the **SQ2** dye-bath required to achieve optimal EQE maxima are 4 hours for the single **SQ2** cell (59.6% at 550 nm, Table 3) *versus* only 20 minutes for the co-sensitized device (59.3% at 670 nm, Table 6). On day 7 after sealing the cell, a value of J_{SC} = 12.26 mA cm^{-2} is obtained for the best performing DSC (Table 6). The V_{OC} increases over a period of 7 days from 493 to 515 mV and the *FF* stays constant. On day 7, a remarkable global efficiency of 4.51% is obtained relative to 6.87% for N719 (Table 6). Setting N719 to 100%, the co-sensitized DSC achieves a relative efficiency of 65.6%. This exceeds the previous record[21] for a copper(I)-based dye (4.66% *versus* 7.36% for N719, equivalent to a relative effciency of 63.3%). Inspection of Table 6 demonstrates that the J_{SC} for the co-sensitized cell is always higher than the DSCs with single dyes. Although the V_{OC} is slightly lower for the co-sensitized *versus* single-dye DSCs, the value of η is always higher, confirming the benefit of co-sensitization. The performance of the DSC was tested again 14 days after assembling the device with the cell being stored in the dark; values of J_{SC}, V_{OC} and η were 12.85 mA cm^{-2}, 534 mV and 4.53%, emphasizing the stability of the device. Inspection of Table S1† reveals that all the DSCs fabricated using the procedure in *Experiment 4* perform well and, in general, their performances improve with time. For example, a co-sensitized DSC assembled by the dipping procedure of *Experiment 4*

(Table 4, **SQ2** concentration of 0.0001 mM in the first dipping step) had a photoconversion efficiency of 4.09% on day 7, 4.01% on day 28 and 3.75% on day 72 after sealing the cell. This again emphasizes the benefits of the dipping procedure of *Experiment 4* and the stability of the co-sensitized DSCs.

Electrochemical impedance spectroscopy (EIS): introduction

Electrochemical impedance spectroscopy (EIS) has become a fundamental tool for investigating the electrochemical properties of DSCs.[22,23,54,55,56,57,58,59] Key parameters that can be determined with the help of fitting circuit models are the recombination resistance (R_{rec}), transport resistance (R_{tr}) and chemical capacitance (C_{μ}). A common way to display the EIS measurements is using a Nyquist plot (Fig. 8).

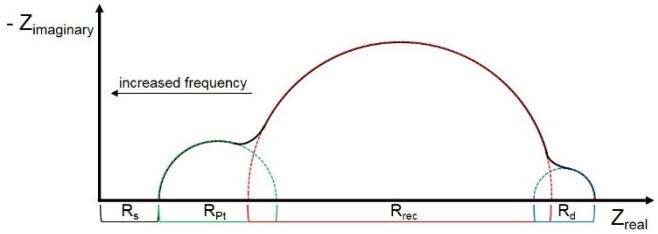

Fig. 8 Schematic representation of a Nyquist plot of a well-functioning DSC at high light intensity with the three semicircles representing the different resistances in a DSC.

Ideally, a Nyquist plot of an EIS measurement on a DSC consists of three semicircles. Depending on the size of each semicircle, they can overlap and may not, therefore, be visible in all measurements. The series resistance (R_s), that arises mainly from the charge transfer resistance of the TiO_2/FTO interface, corresponds to the value of the lowest interception of the first semicircle that rises from the cathode/electrolyte charge transfer resistance (R_{Pt}). The second semicircle is the recombination resistance of the interaction of the TiO_2/dye/electrolyte interface (R_{rec}). The last semicircle at low frequencies gives the diffusion resistance of the charge carrier particles in the electrolyte (R_d). In order to extract these parameters from the measurement, two different equivalent circuit models were used. At higher light intensities, a model with two Randles-type circuits were used for EIS measurements at 22 mW cm^{-2} light intensity ().[60] The fitting model consists of two Randles-type circuits in series and a further series resistance (R_s). An additional Warburg diffusion element (Ws) has been introduced. Each circuit characterizes one electrode interface. The first circuit models the electrolyte/Pt/FTO interface and the second one the TiO_2/dye/electrolyte interface.

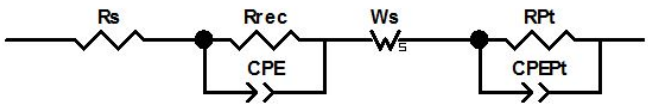

Fig. 9 Fitting model for EIS measurements at a light intensity of 22 mW cm^{-2}.

The fitting of the EIS measurements at a light intensity of 2.2 mW cm^{-2} were performed with a model (Fig. 10) that was discussed in detail in an earlier publication.[22] It consists of an extended distributed element (DX) to fit the TiO_2/dye/electrolyte interface according to the transition line model.[61] With this extended distributed element, it is possible to establish R_{tr}. The Warburg diffusion element (Ws) is again used to model the diffusion impedance of the charge carrier through the electrolyte close to the active surface. The Randles-type circuit containing R_{Pt} and CPE_{Pt} models the Pt counter electrode. The series resistance of the whole measurement is modeled by a series resistance (*Rs*).

Fig. 10 Fitting model for EIS measurements at a light intensity of 2.2 mW cm^{-2}.

The following discussion compares single-dye DSCs containing [Cu(**3**)(**1**)]$^+$ or **SQ2**, and then considers the EIS results of the co-sensitized DSC with the best dipping procedure (*Experiment 4*, Table 4) in comparison to the single-dye DSCs. The EIS measurements were conducted on DSCs that had aged for 3 days.

EIS measurements

We have already discussed EIS data for a DSC containing the dye [Cu(**3**)(**1**)]$^+$,[22] and the EIS parameters of this DSC are comparable with those of other copper(I) DSCs.[22,23,57,59] A single-dye **SQ2** DSC has been investigated by EIS by Fang *et al*.[38] and values of R_{rec} = 24.7 Ω and the electron lifetime τ = 11.2 ms were reported. These data are comparable with the EIS parameters measured at a light intensity of 22 mW cm^{-2} in this study (R_{rec} = 25.5 Ω, τ = 8.1 ms, Table 7). The low R_{rec} is a well-known disadvantage of organic DSCs and is one of the most crucial issues that needs to be addressed for organic DSCs in order to improve their performances.[62,63,64,65,66,67]

Table 7 EIS data obtained from measurements at a light intensity of 22 mW cm^{-2} of DSCs containing the dye Cu[(**3**)(**1**)]$^+$, **SQ2** (dipping time 20 min) or the co-sensitization of both dyes by the best dipping procedure (see text).

Dye	R_{rec} [Ω]	C_{μ} [μF]	R_{Pt} [Ω]	$C_{Pt\mu}$ [μF]	τ^a [ms]
[Cu(**3**)(**1**)]$^+$	178.8	319.4	30.6	16.3	57.1
SQ2	25.5	316.7	40.7	9.8	8.1
co-sens. DSC	24.2	362.4	10.4	12.1	8.8

[a] $\tau = R_{rec}C'$; $C' = (R_{rec}{}^{1-n}C)^{1/n}$ where n = constant phase element factor and C' = corrected C.[68]

A comparison of the EIS data (Table 7) for the [Cu(**3**)(**1**)]$^+$ and **SQ2** DSCs at a light intensity of 22 mW cm^{-2} shows that the C_{μ} is almost the same for both DSCs, but the R_{rec} is much higher for the DSC containing [Cu(**3**)(**1**)]$^+$. The longer electron lifetime, τ, observed for [Cu(**3**)(**1**)]$^+$ versus **SQ2** or the co-sensitized DSC (Table 7) is consistent with the much higher value of R_{rec} which militates against back reactions of the electrons in the conductance band. To obtain the transport

resistance (R_{tr}), EIS measurements at low light intensity are required, and the fitted EIS parameters at a light intensity of 2.2 mW cm^{-2} are shown in Table 8. The Nyquist plots at light intensities 22 and 2.2 mW cm^{-2} are shown in Fig. S10†. R_{tr} for the DSC sensitized by [Cu(**3**)(**1**)]$^+$ is considerably higher than for **SQ2**. This is consistent with the lower spectral response of the copper-based dye which leads to a lower number of absorbed photons.

Table 8 EIS data obtained from measurements at a light intensity of 2.2 mW cm^{-2} of DSCs containing the dye Cu[(**3**)(**1**)]$^+$, **SQ2** (dipping time 20 min) or the co-sensitization of both dyes by the best dipping procedure (see text).

dye	R_{rec} [Ω]	C_{μ} [μF]	R_{Pt} [Ω]	$C_{Pt\mu}$ [μF]	R_{tr} [Ω]	τ [ms]	L_d [μm]
[Cu(**3**)(**1**)]$^+$	893.3	186.7	19.4	7.2	105.9	166.7	34.9
SQ2	141.8	224.3	36.0	7.7	46.3	31.8	21.0
co-sens. DSC	151.0	195.3	10.6	8.6	50.3	29.5	20.8

An informative parameter to describe the interplay between R_{rec} and R_{tr} is the length of diffusion (L_d) which is calculated according to eqn. 1.[61]

$$L_D = L\sqrt{\frac{R_{rec}}{R_{tr}}} \quad (1)$$

Although R_{rec} for the **SQ2** DSC is low (Table 7), it is a well performing cell, because R_{tr} must also to be taken into account. An efficient charge injection requires an L_d larger than the thickness of the semiconductor (here L ~12 μm). As a consequence, when the ratio of R_{rec} to R_{tr} is greater than unity, the length of diffusion is long enough to minimize back reactions due to a long charge transit time. In this study, the DSCs containing [Cu(**3**)(**1**)]$^+$ or **SQ2** both have an L_d two to three times larger than L.

When comparing the EIS measurements of the co-sensitized DSC with the single-dye DSCs (Tables 7 and 8), it is observed that its characteristics resemble those of a pristine **SQ2** DSC. All parameters at a light intensity of 22 mW cm^{-2} are comparable to the single-dye **SQ2** DSC. The co-sensitized DSC has the highest C_{μ} of all the DSCs in this study. At the counter-electrode of the co-sensitized DSC, a low R_{Pt} is observed which enhances the charge transition at the cathode/electrolyte interface. R_{tr} for the co-sensitized DSC is as low as in the single-dye **SQ2** DSC. We note that **SQ2** can also partly bind to the scattering layer of the working electrode of the DSC in the single- and co-sensitized DSC; the evidence for this is that the scattering layer only becomes coloured when the electrode is exposed to **SQ2**. Because of the cell architecture, **SQ2** adsorbed on the scattering layer can come in contact with the electrolyte and this may be a reason why R_{rec} is lower for the DSC containing the **SQ2**. In conclusion, an optimal electron transport in the DSC is promoted by an interplay of the parameters discussed above and as a consequence, the highest J_{SC} is observed for the co-sensitized DSC. Additionally, L_d (Table 8) is almost twice the magnitude of L which is an appropriate value for a well performing DSC.

Filter tests with a single-dye SQ2 DSC and a co-sensitized DSC

Light filter tests were performed in order to investigate whether the two dyes in the co-sensitized DSC work independently or via an electron or energy transfer mechanism.[69] The *J-V* curves and EQE spectra were recorded with filters in place to block light in particular wavelength ranges. Two filters with specific light transmittance were chosen: a 500 nm short-pass filter and a 550 nm long-pass filter (Fig. 11). The 500 nm short-pass filter blocks light with a wavelength longer than 500 nm. The 550 nm long-pass filter blocks light with a wavelength shorter than 550 nm. Additional measurements with a 41% transmittance filter were performed to investigate the performance at reduced light intensities; a 41% transmittance filter was the available filter closest to 50%. For the filter tests, the best-performing **SQ2** cell (dipping time of 4 hours, Table 3) and a co-sensitized DSC assembled by the procedure in *Experiment 4* (Table 4) with 0.0001 mM **SQ2** (DSC number 2 in Table S1†) were used. The measurements were performed as described in the Experimental section. The different irradiances in Table 9 were obtained by placing the respective filters on top of a fully-masked Si reference photodiode.

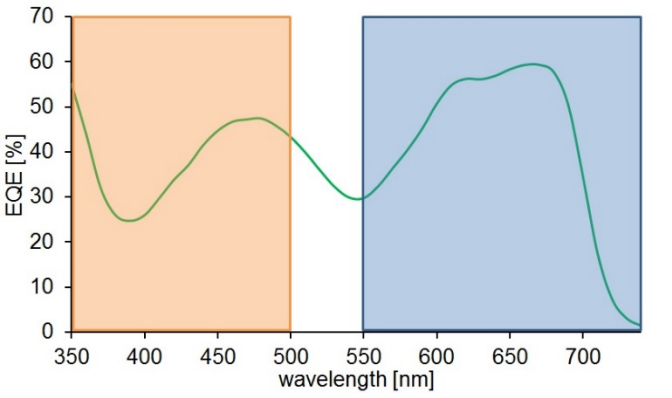

Fig. 11 Transmittance range of the 500 nm short-pass (orange rectangle) and 550 nm long-pass (blue rectangle) filters with respect to the EQE spectrum of the measured co-sensitized DSC.

Fig. 12 displays the *J-V* curves of the DSCs without or with the filters. Both DSCs have a value of η > 3% without a filter (3.75% for the co-sensitized DSC and 3.36% for the single-dye **SQ2** DSC, Table 9). Inspection of Fig. 12 and Table 9 demonstrates the fact that both DSCs have comparable J_{SC} values with a 550 nm long-pass filter (4.97 mA cm^{-2} for the co-sensitized DSC and 5.07 mA cm^{-2} for the single-dye **SQ2** DSC, Table 9). At reduced light intensity achieved by placing a 41% transmittance filter on top of the 550 nm long-pass filter (Table 9), the same J_{SC} values were observed for the co-sensitized DSC (2.12 mA cm^{-2}) and the single-dye **SQ2** DSC (2.11 mA cm^{-2}). This demonstrates that a dipping time of 20 minutes with respect to 4 hours for the single-dye DSC are adequate to obtain optimal performance of the **SQ2** dye in the co-sensitized DSC.

Table 9 Performance parameters and EQE maxima of a co-sensitized DSC assembled by the dipping procedure of *Experiment 4* and of a single-dye DSCs containing the dye **SQ2** with a dipping time of 4 hours without a filter, a 550 nm long-pass filter with or without additional 41% transmittance filter and a 500 nm short-pass filter

Dye	filter	irradiance[a] [mW cm^{-2}]	J_{SC} [mA cm^{-2}]	V_{OC} [mV]	*FF* [%]	η [%]	EQE max [nm], [%]	
co-sens. DSC	no filter	100	9.71	552	70.0	3.75	460, 37.3	660, 42.6
SQ2	no filter	100	8.37	563	71.3	3.36		550, 43.2
co-sens. DSC	550	69.2	4.97	536	72.1	2.78		670, 41.6
SQ2	550	69.2	5.07	556	72.0	2.93		550, 43.9
co-sens. DSC	550/41% light	30.8	2.12	516	72.4	2.57		670, 15.7
SQ2	550/41% light	30.8	2.11	534	72.5	2.66		570, 15.5
co-sens. DSC	500	8.3	1.30	468	74.2	5.46	460, 35.7	

a) irradiance values obtained with a fully-masked Si reference cell and the corresponding filters placed on top (Experimental section).

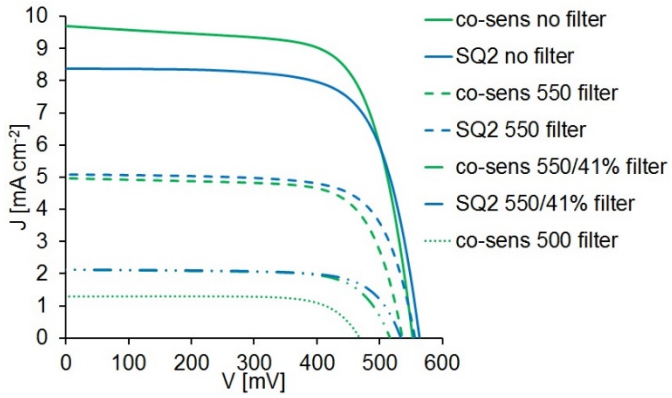

Fig. 12 *J-V* curves of a co-sensitized DSC and a single-dye **SQ2** DSC without filter, with a 550 nm long-pass filter with and without additional 41% transmittance filter and with a 500 nm short-pass filter.

The performance of the co-sensitized DSC with a 500 nm short-pass filter shows that the copper(I)-dye performs well under reduced light intensity (Table 9). The impact of the light intensity on the overall efficiency η is presented in eqn. 2. The key parameters leading to improved efficiency at lower light intensities are J_{SC}, V_{OC} and *FF*.

$$\eta = \frac{J_{sc} \cdot V_{oc} \cdot FF}{P_{in}} \cdot 100\% \qquad (2)$$

The impact of the light intensity on V_{OC} is observed in the filter measurements. The lower the light intensity, the lower the V_{OC}, consistent with previous investigations.[70,71,72,73,74,75] The co-sensitized DSC without a filter has V_{OC} = 552 mV (Table 9) which decreases at lower light intensity: at a light intensity of 69.2 mW cm^{-2}, V_{OC} = 536 mV, while at 30.8 mW cm^{-2} , V_{OC} = 516 mV and at 8.3 mW cm^{-2} it is 486 mV. This is consistent with the linear relationship between V_{OC} and the logarithm of the light intensity (Fig. S11).[70,71,72] As a control experiment, the EQE spectra of a single-dye **SQ2** cell with and without a 550 nm long-pass filter were measured and are shown in Fig. 13. Within the transmittance range of the filter, identical EQE responses are obtained in both experiments. The same filter tests were performed with the co-sensitized DSC (Fig. 14). Firstly, the EQE measurement with a 500 nm short-pass filter resulted in a slightly lower EQE response than without the filter. This is mainly due to the lower number of incident photons. Because of the properties of the filters, an EQE measurement with a reference to the 500 nm short-pass filter was not possible. A measurement with a 550 nm long-pass filter gave a comparable EQE spectrum with respect to that without the filter (Fig. 14). Differences between values of EQE_{max} with and without the filter were ≤1%. The validation of the measurements was obtained using both the 500 nm short-pass and the 550 nm long-pass filters which gave a negligible EQE response (purple trace in Fig. 14), confirming that there was no background response due to the bias light.

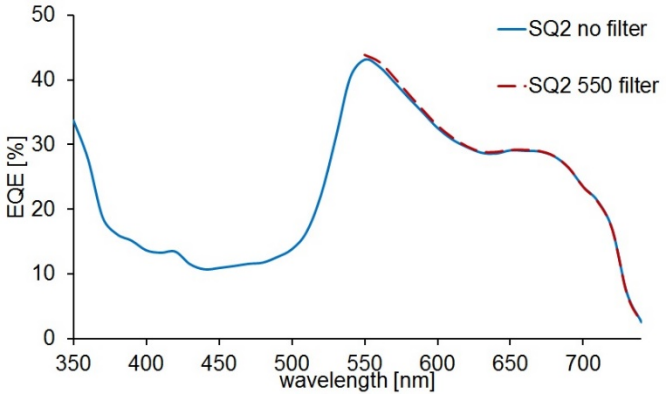

Fig. 13 EQE curve of a single-dye **SQ2** DSC with and without a 550 nm long-pass filter at the transmittance range of the filter.

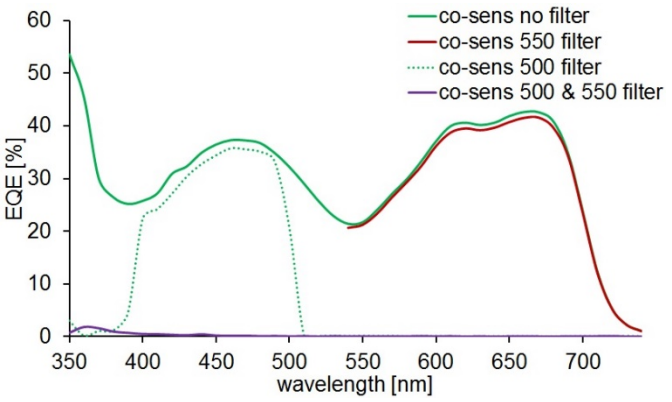

Fig. 14 EQE curve of a co-sensitized DSC without a filter, with a 550 nm long-pass filter at the transmittance range of the filter, with a 500 nm short-pass filter and with both filters.

The results of EQE measurements carried out with the filters are consistent with the two dyes operating independently. For efficient electron injection, the lowest unoccupied orbitals (LUMOs) should be localized on the anchoring domain of the dye. DFT calculations previously reported for **SQ2**[41] show that this dye has a LUMO localized on the anchoring unit. Ground state DFT calculations were carried out on [Cu(**3**)(**1**)]$^+$ with the geometry optimized at the PM3 level. We chose a 6-31G* basis set on all atoms, since we have previously demonstrated that the orbital characteristics are basically unaltered by using larger basis sets, even though calculated absorption spectra are significantly influenced.[76] The highest occupied and lowest unoccupied orbitals of [Cu(**3**)(**1**)]$^+$ are shown in Fig. 15, and show that the LUMO manifold contains orbitals with significant anchor character. Thus, the orbital characteristics are compatible with both dyes being able to inject electrons in contrast to other investigated co-sensitized DSCs where an electron transfer mechanism may be operative.[69]

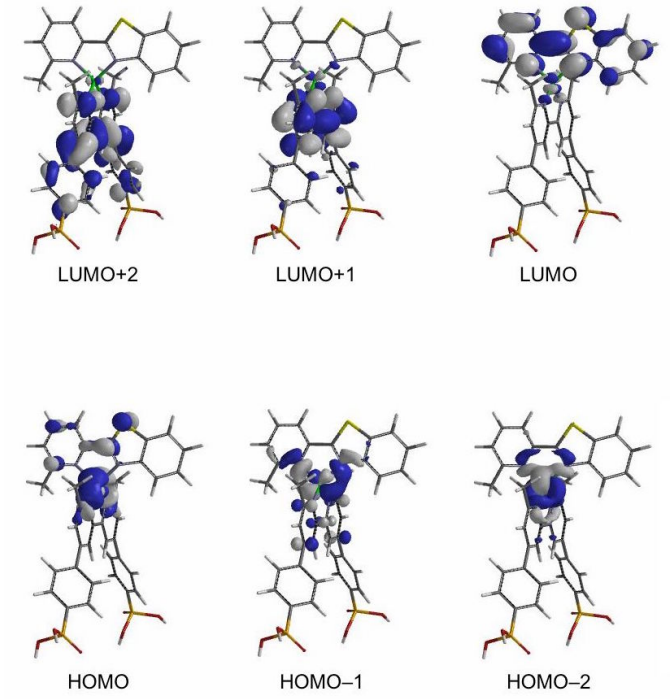

Fig. 15 The frontier molecular orbitals of [Cu(**3**)(**1**)]$^+$ at B3LYP/6-31G* level (gas phase, ground state).

Conclusions

We have described the first example of co-sensitization in DSCs using a copper(I)-based sensitizer and a commercially available organic dye. By judicious matching of the EQE maxima arising from the heteroleptic copper(I) dye [Cu(**3**)(**1**)]$^+$ and from organic dye **SQ2** in complementary parts of the visible spectrum, we have achieved the highest photoconversion efficiency reported for a copper-based DSC (65.6% relative to N719 set at 100%). This result confirms the potential for the use of Earth-sustainable copper as the basis of sensitizers in DSCs.

The investigation has shown that the sequences in which the photoanodes of the n-type DSCs are exposed to [Cu(**3**)(**1**)]$^+$ and **SQ2**, and the times that the electrodes are immersed in the respective dye baths, critically influence the overall performance of the DSCs. Aggregation of the **SQ2** molecules on the electrode surface is important in terms of achieving panchromatic light-harvesting of the co-sensitized DSCs, but excessive aggregation is detrimental. The results of EQE measurements carried out with different wavelength-range filters are consistent with the two dyes operating independently.

Acknowledgements

We acknowledge the Swiss National Science Foundation (Grant number 200020_162631), the Swiss Nanoscience Institute (for the purchase of the EIS instrument) and the University of Basel for financial support.

Notes and references

1 M. Grätzel, *Acc. Chem. Res.*, 2009, **42**, 1788; M. Grätzel, *Inorg. Chem.*, 2005, **44**, 6841; M. Grätzel, *J. Photochem. Photobiol. C*, 2003, **4**, 145 and references therein.
2 K. Kalyanasundaram, ed., *Dye Sensitized Solar Cells*, 2010, CRC Press, Boca Raton.
3 B. O'Regan and M. Grätzel, *Nature*, 1991, **353**, 737.
4 A. Mishra, M. Fischer and P. Bäuerle, *Angew. Chem. Int. Ed.*, 2009, **48**, 2474.
5 A. Yella, H.-W. Lee, H. N. Tsao, C. Yi, A. K. Chandiran, M. K. Nazeeruddin, E. W.-G. Diau, C.-Y. Yeh, S. M. Zakeeruddin and M. Grätzel, *Science*, 2011, **334**, 629.
6 T. Higashino and H. Imahori, *Dalton Trans.*, 2015, **44**, 448.
7 A. Hagfeldt, G. Boschloo, L. Sun, L. Kloo and H. Pettersson, *Chem. Rev.*, 2010, **110**, 6595.
8 Y. Xie, Y. Tang, W. Wu, Y. Wang, J. Liu, X. Li, H. Tian and W.-H. Zhu, *J. Am. Chem. Soc.*, 2015, **137**, 14055.
9 H. Ozawa, Y. Okuyama and H. Arakawa, *ChemPhysChem*, 2014, **15**, 1201.
10 K. Kakiage, Y. Aoyama, T. Yano, T. Otsuka, T. Kyomen, M. Unno and M. Hanaya, *Chem. Commun.*, 2014, **50**, 6379.
11 C.-Y. Chen, M. Wang, J.-Y. Li, N. Pootrakulchote, L. Alibabaei, C-ha Ngoc-le, J.-D. Decoppet, J.-H. Tsai, C. Grätzel, C.-G. Wu, S. M. Zakeeruddin and M. Grätzel, *ACS Nano*, 2009, **3**, 3103.
12 S. Mathew, A. Yella, P. Gao, R. Humphry-Baker, B. F. E. Curchod, N. Ashari-Astani, I. Tavernelli, U. Rothlisberger, Md. K. Nazeeruddin and M. Grätzel, *Nature Chem.*, 2014, **6**, 242

13 K. Kakiage, Y. Aoyama, T. Yano, K. Oya, T. Kyomen and M. Hanaya, *Chem. Commun*., 2015, **51**, 6315.
14 Z. Yao, M. Zhang, H. Wu, L. Yang, R. Li and P. Wang, *J. Am. Chem. Soc.*, 2015, **137**, 3799.
15 K. Kakiage, Y. Aoyama, T. Yano, K. Oya, J-i. Fujisawa and M. Hanaya, *Chem. Commun.*, 2015, **51**, 15894.
16 B. Bozic-Weber, E.C. Constable and C.E. Housecroft, *Coord. Chem. Rev.*, 2013, **257**, 3089.
17 C.E. Housecroft and E.C. Constable, *Chem. Soc. Rev.*, 2015, **44**, 8386.
18 M. Sandroni, Y. Pellegrin and F. Odobel, *C. R. Chimie*, 2016, **19**, 79
19 M. Magni, P. Biagini, A. Colombo, C. Dragonetti, D. Roberto and A. Valore, *Coord. Chem. Rev.*, 2016, **322**, 69.
20 F. J. Malzner, S. Y. Brauchli, E. C. Constable, C. E. Housecroft and M. Neuburger, *RSC Adv*., 2014, **4**, 48712.
21 M. Sandroni, L. Favereau, A. Planchat, H. Akdas-Kilig, N. Szuwarski, Y. Pellegrin, E. Blart, H. Le Bozec, M. Boujtita and F. Odobel, *J. Mater. Chem. A*, 2014, **2**, 9944.
22 F. J. Malzner, C. E. Housecroft, E. C. Constable and M.Willgert, *J. Mater. Chem. A*., 2017, **5**, 4671.
23 S. O. Fürer, B. Bozic-Weber, T. Schefer, C. Wobill, E. C. Constable, C. E. Housecroft and M. Willgert, *J. Mater. Chem. A*, 2016, **4**, 12995.
24 B. Bozic-Weber, S. Y. Brauchli, E. C. Constable, S. O. Fürer,C. E. Housecroft and I. A. Wright, *Phys. Chem. Chem. Phys*., 2013, **15**, 4500.
25 S. Y. Brauchli, F. J. Malzner, E. C. Constable and C. E. Housecroft, *RSC Adv*.,2015, **5**, 48516.
26 B. Bozic-Weber, E. C. Constable, S. O. Fürer, C. E. Housecroft, L. J. Troxler and J. A. Zampese, *Chem. Commun*., 2013, **49**, 7222.
27 M. Sandroni, M. Kayanuma, A. Planchat, N. Szuwarski, E. Blart, Y. Pellegrin, C. Daniel, M. Boujtitaa and F. Odobel, *Dalton Trans*., 2013, **42**, 10818.
28 M. Sandroni, M. Kayanuma, M. Rebarz, H. Akdas-Kilig, Y. Pellegrin, E. Blart, H. Le Bozec, C. Daniel and F. Odobel, *Dalton Trans.*, 2013, **42**, 14628.
29 J.-H. Yum, E. Baranoff, S. Wenger, M. K. Nazeeruddin and M. Grätzel, *Energy Environ. Sci.*, 2011, **4**, 842.
30 D. D. Babu, D. Elsherbiny, H. Cheema, A. El-Shafei and A. V. Adhikari, *Dyes and Pigments*, 2016, **132**, 316.
31 S. Chang, H. Wang, L. T. L. Lee, S. Zheng, Q. Li, K. Y. Wong, W.-K. Wong, X. Zhu, W.-Y. Wong, X. Xiao and T. Chen, *J. Mater. Chem. C*, 2014, **2**, 3521.
32 J.-H. Yum, S.-R. Jang, P. Walter, T. Geiger, F. Nüesch, S. Kim, J. Ko, M. Grätzel and M. K. Nazeeruddin, *Chem. Commun*., 2007, 4680.
33 Y. Zhao, F. Lu, J. Zhang, Y. Dong, B. Zhang and Y. Feng, *RSC Adv*., 2017, **7**, 10494.
34 J. Chang, C.-P. Lee, D. Kumar, P.-W. Chen, L.-Y. Lin, K.R. J. Thomas and K.-C. Ho, *J. Power Sources*, 2013, **240**, 779.
35 L.-Y. Lin, M.-H. Yeh, C.-P. Lee, J. Chang, A. Baheti, R. Vittal, K.R. J. Thomas and K.-C. Ho, *J. Power Sources*, 2014, **247**, 906.
36 R. Y.-Y. Lin, H.-W. Lin, Y.-S. Yen, C.-H. Chang, H.-H. Chou, P.-W. Chen, C.-Y. Hsu, Y.-C. Chen, J. T. Lin and K.-C. Ho, *Energy Environ. Sci*., 2013, **6**, 2477.
37 Z. Xue, L. W. and B. Liu, *Nanoscale*, 2013, **5**, 2269.
38 M. Fang, H. Li, Q. Li and Z. Li, *RSC Adv*., 2016, **6**, 40750.
39 M. Rudolph, T. Yoshida, H. Miura and D. Schlettwein, *J. Phys. Chem. C*, 2015, **119**, 1298.
40 R. Y.-Y. Lin, Y.-S. Yen, Y.-T. Cheng, C.-P. Lee, Y.-C. Hsu, H.-H. Chou, C.-Y. Hsu, Y.-C. Chen, J. T. Lin, K.-C. Ho and C. Tsai, *Org. Lett*., 2012, **14**, 14, 3612.
41 T. Geiger, S. Kuster, J.-H. Yum, S.-J. Moon, M. K. Nazeeruddin, M. Grätzel and F. Nüesch, *Adv. Funct. Mater*. 2009, **19**, 2720.
42 S. G. Hashmi, M. Özkan, J. Halme, S. M. Zakeeruddin, J. Paltakari, M. Grätzel and P. D. Lund, *Energy Environ. Sci*., 2016, **9**, 2453.
43 B. Bozic-Weber, S. Y. Brauchli, E. C. Constable, S. O. Fürer, C. E. Housecroft, F. J. Malzner, I. A. Wright and J. A. Zampese, *Dalton Trans*., 2013, **42**, 12293.
44 H. J. Snaith, *Energy Environ. Sci*., 2012, **5**, 6513.
45 H. J. Snaith, *Nat. Photonics*, 2012, **6**, 337.
46 S. Y. Brauchli, F. J. Malzner, E. C. Constable and C. E. Housecroft, *RSC Adv.*, 2014, **4**, 62728.
47 L. Zhang and J. M. Cole, *ACS Appl. Mater. Interfaces*, 2015, **7**, 3427.
48 A. Abate, R. Pérez-Tejada, K. Wojciechowski, J. M. Foster, A. Sadhanala, U. Steiner, H. J. Snaith, S. Franco and J. Orduna, *Phys. Chem. Chem. Phys.,* 2015, **17**, 18780.
49 C. O'Rourke and D. R. Bowler, *J. Phys.: Condens. Matter*, 2014, **26**, 195302.
50 R. Luschtinetz, S. Gemming and G. Seifert, *Eur. Phys. J. Plus*, 2011, **126**, 98.
51 B. Wenger, M. Grätzel and J.-E. Moser*, J. Am. Chem. Soc*., 2005, **127**, 12150.
52 B. Wenger, M. Grätzel and J.-E. Moser, *Chimia*, 2005, **59**, 123.
53 V. K. Thorsmølle, B. Wenger, J. Teuscher, C. Bauer and J.-E. Moser, *Chimia*, 2007, **61**, 631.
54 F. Fabregat-Santiago, G. Garcia-Belmonte, I. Mora-Sero and J. Bisquert, *Phys. Chem. Chem. Phys*., 2011, **13**, 9083.
55 J. Bisquert, *J. Electroanal. Chem*., 2010, **646**, 43.
56 F. Fabregat-Santiago, J. Bisquert, E. Palomares, L. Otero, D. Kuang, S. M. Zakeeruddin and M. Grätzel, *J. Phys. Chem. C*, 2007, **111**, 6550.
57 Y. Baumgartner, Y. M. Klein, E. C. Constable, C. E. Housecroft and M. Willgert, *RSC Adv*., 2016, **6**, 86220.
58 M. Willgert, A. Boujemaoui, E. Malmström, E. C. Constable and C. E. Housecroft, *RSC Adv*., 2016, **6**, 56571.
59 Y. M. Klein, M. Willgert, A. Prescimone, E. C. Constable and C. E. Housecroft, *Dalton Trans*., 2016, **45**, 4659.

60 S. Carli, E. Benazzi, L. Casarin, T. Bernardi, V. Bertolasi, R. Argazzi, S. Caramori and C.A. Bignozzi, *Phys. Chem. Chem. Phys*., 2016, **18**, 5949.
61 Q. Wang, S. Ito, M. Grätzel, F. Fabregat-Santiago, I. Mora-Sero, J. Bisquert, T. Bessho and H. Imai, *J. Phys. Chem. B,* 2006**, 110***,* 25210.
62 A. Mishra, M. K. R. Fischer and P. Bäuerle, *Angew. Chem. Int. Ed*., 2009, **48**, 2474.
63 S. Ito, T. N. Murakami, P. Comte, P. Liska, C. Grätzel, M. K. Nazeeruddin, M. Grätzel, *Thin Solid Films*, 2008, **516**, 4613.
64 M. Miyashita, K. Sunahara, T. Nishikawa, Y. Uemura, N. Koumura, K. Hara, A. Mori, T. Abe, E. Suzuki and S. Mori, *J. Am. Chem. Soc*., 2008, **130**, 17874.
65 E. M. Barea, C. Zafer, B. Gultekin, B. Aydin, S. Koyuncu, S. Icli, F. Fabregat Santiago and J. Bisquert, *J. Phys. Chem. C*, 2010, **114**, 19840.
66 A. J. Huckaba, A. Yella, P. Brogdon, J. S. Murphy, M. K. Nazeeruddin, M. Grätzel and J. H. Delcamp, *Chem. Commun.,* 2016, **52**, 8424.
67 H.-H. Chou, C.-H Yang, J. T. Lin and C.-P. Hsu, *J. Phys. Chem. C*, 2017, **121**, 983.
68 M.R. Shoar Abouzari, F. Berkemeier, G. Schmitz and D. Wilmer, *Solid State Ionics*, 2009, **180**, 922; J. Bisquert, F. Fabregat-Santiago, I. Mora-Seró, G. Garcia-Belmonte and S. Giménez, *J. Phys. Chem. C*, 2009, **113**, 17278.
69 K. Kakiage, Y. Aoyama, T. Yano, K. Oya, J.-I. Fujisawa and M. Hanaya, *Chem. Commun.*, 2015, **51**, 15894.
70 C. M. Ramsdale, J. A. Barker, A. C. Arias, J. D. MacKenzie, R. H. Friend and N. C. Greenham, *J. Appl. Phys*., 2002, **92**, 4266.
71 L. J. A. Koster, V. D. Mihailetchi, R. Ramaker and P. W. M. Blom, *Appl. Phys. Lett*., 2005, **86**, 123509.
72 P. Salvador, M. Gonzalez Hidalgo, A. Zaban and J. Bisquert, *J. Phys. Chem. B*, 2005, **109**, 15915.
73 P. R. F. Barnes, A. Y. Anderson, J. R. Durrant and B. C. O'Regan, *Phys. Chem. Chem. Phys*., 2011, **13**, 5798.
74 J. A. Barker, C. M. Ramsdale, and N. C. Greenham, *Phy. Rev. B*, 2003, **67**, 075205.
75 H. J. Snaith, L. Schmidt-Mende and M. Grätzel, *Phy. Rev. B*, 2006, **74**, 045306.
76 B. Bozic-Weber, V. Chaurin, E. C. Constable, C. E. Housecroft, M. Meuwly, M. Neuburger, J. A. Rudd, E. Schönhofer and L. Siegfried, *Dalton Trans*., 2012, **41**, 14157.